Downloaded from specialpapers.gsapubs.org on November 29, 2014

The Geological Society of America
Special Paper 509
2015

Behavior and damage of the Washington Monument during the 2011 Mineral, Virginia, earthquake

S. Golnaz Shahidi
Shamim N. Pakzad
James M. Ricles
Department of Civil and Environmental Engineering, Lehigh University, Bethlehem, Pennsylvania 18015, USA

James R. Martin
Department of Civil Engineering, Clemson University, Clemson, South Carolina 29634, USA

C. Guney Olgun
Elizabeth A. Godfrey
Department of Civil and Environmental Engineering, Virginia Polytechnic Institute and State University, Blacksburg, Virginia 24061, USA

ABSTRACT

This paper investigates the potential causes of the damage to the Washington Monument sustained from the 2011 Mineral, Virginia (USA), earthquake through time-history dynamic analysis. Ambient vibration field test data were obtained and utilized to calibrate a finite element model of the structure and its foundation. The impact of the foundation modeling and the uncertainties associated with the material properties of the stone and iron, in the absence of in situ material testing, were investigated through several parametric studies, in which the material property values are permuted at three (upper, average, and lower) levels to bound the predicted dynamic characteristics of the structure. Because ground-motion data recorded in the Washington, D.C., area during the earthquake are scarce, the ground motion at the Washington Monument site was simulated using an angular transformation of the recorded ground motions in Reston, Virginia, deconvoluted to the bedrock level and upward propagation of the rotated motions to the ground surface based on soil profiles in Reston and the Washington Monument site provided by the U.S. Geological Survey. The finite element model of the Washington Monument shaft subjected to these bidirectional earthquake records showed high acceleration amplification at the observation level, as well as tensile stress concentration at the ~107 m level. These observations correlate with the damage observed in the pyramidion section and upper levels of the Washington Monument shaft following the 2011 Virginia earthquake.

Shahidi, S.G., Pakzad, S.N., Ricles, J.M., Martin, J.R., Olgun, C.G., and Godfrey, E.A., 2015, Behavior and damage of the Washington Monument during the 2011 Mineral, Virginia, earthquake, *in* Horton, J.W., Jr., Chapman, M.C., and Green, R.A., eds., The 2011 Mineral, Virginia, Earthquake, and Its Significance for Seismic Hazards in Eastern North America: Geological Society of America Special Paper 509, doi:10.1130/2015.2509(13). For permission to copy, contact editing@geosociety.org. © 2014 The Geological Society of America. All rights reserved.

Downloaded from specialpapers.gsapubs.org on November 29, 2014

INTRODUCTION: THE 2011 VIRGINIA EARTHQUAKE

The Virginia earthquake of 23 August 2011, had a moment magnitude, M_w, of 5.8 and was the largest historical earthquake in the Central Virginia seismic zone and the largest in Virginia since the 1897 Giles County earthquake. According to the U.S. Geological Survey (USGS), the perceived intensity of this widely felt ground motion was "very strong" in the epicenter area (Mineral, Virginia), and "moderate" in the Washington, D.C., area. In spite of the lower level of intensity in Washington, D.C., the Washington Monument was extensively damaged during this earthquake. The extent of the observed damage, including cracks, surface spalling, and dislodging of stone blocks in the pyramidion, crumbled mortar, and damage to the elevator, forced the immediate evacuation of the structure, and public access was suspended until adequate repairs to the interior and the exterior of the structure were completed. Being a structure of national historical significance, as well as the world's tallest obelisk, there is a substantial interest in understanding the causes of the damage developed in this structure during the earthquake.

As an attempt toward this goal, this paper explores the impact of the 2011 Virginia earthquake on the Washington Monument using finite element modeling and time-history analysis. A finite element model (FEM) of the masonry shaft of the Washington Monument (WAMO) was developed based on the structure's blueprints. Due to lack of detailed information related to the material properties of the structure, a number of assumptions are made and the impact of such assumptions on the structural vibration characteristics is investigated. In order to minimize the modeling uncertainties, the ambient vibration of the WAMO was monitored and the modal quantities are identified. The FEM with the closest modal parameters to the identified modes is then subjected to the simulated ground shaking at the WAMO site during the Virginia earthquake. The response of this model to the simulated earthquake is investigated to explain the causes of the inflicted damage to this structure.

This paper is organized as follows. We first review the construction history of the WAMO and the summary of the observed damage in this structure through different condition surveys. Subsequently, the modeling of the substructure and superstructure of the WAMO is described in detail. We then describe the ambient vibration field test conducted on the WAMO and the procedure for ground shaking estimation at its location based on the recorded motions at the nearest station. Results of a response spectrum study using analytically and experimentally identified modal quantities and ground motion time-history analysis are presented and possible causes of the observed damage in this structure are discussed. We conclude with a summary of the findings of this research.

PHYSICAL DESCRIPTION OF THE WASHINGTON MONUMENT

The construction history of the WAMO is briefly described based on a historic blueprint of this structure found on the Library of Congress website (Historic American Engineering Record, 1986).

The masonry shaft of the WAMO (shown in Fig. 1) can be divided into four basic sections. The first section consists of walls made of marble and bluestone that extend vertically from a stair-stepped pyramid foundation made of blue gneiss. This section was constructed in 1848 after the establishment of the National Monument Society, which solicited public funding for the construction of the monument. Due to setbacks in securing funding and the onset of the Civil War, construction was halted for more than two decades. At this point, the construction of the WAMO was given to the U.S. Army Corps of Engineers. A study done by Colonel Thomas L. Casey at the time indicated that the original foundation would not be sufficient to support the massive weight of the WAMO (John Milner Associates, Inc., 2004). Therefore, the foundation was redesigned and strengthened using a system of tunneling and filling with concrete. The new foundation, with a base 38.5 m long at each side and a depth of 11.2 m, fully encased the primary foundation in concrete (John Milner Associates, Inc., 2004). Casey based the new design of the masonry shaft of the WAMO on architectural concepts of the Egyptian obelisks. Therefore, in the final design, the outer walls are tapered by 0.64 cm per 30.5 cm (Historic American Engineering Record, 1986) and the WAMO is 169.3 m tall, including its pyramidion; the height of the structure is approximately 10 times its baseline dimension of 16.9 m. The second section of the monument, from elevation 45.7 m to 48.8 m, was built when construction resumed after the final designs were completed. This section is important because within it the inner walls are not vertical and the inner dimensions of the structure change from 7.6 m to 9.6 m. The third section of the WAMO extends from 48.8 m to 152.4 m just below the pyramidion. This section is similar to the first section, the changes being the dimensions and thickness of the walls and the type of stone used in their construction (marble and granite below the 137.2 m level, and marble from the 137.2 m to 152.4 m level). The fourth section of the WAMO is the pyramidion, from 152.4 m to 169.3 m. An aluminum cap is at the tip of the pyramidion to protect the stone from weathering.

This historic blueprint was also able to provide some information regarding the inner structure of the monument. Horizontal platforms and staircases that are shown in Figure 1 are located at every 3.05 m along the height of the structure. Vertical columns support the platforms, staircase, and an elevator shaft which is in the center of the monument. More detailed blueprints of the interior structure are available through the National Park Service (Oehrlein and Associates Architects, 1993). Shown in Figure 2 are interior sections of the WAMO at 45.7 m and 48.8 m levels. This figure shows that there are eight columns (circled in Fig. 2) extending vertically over the height

Downloaded from specialpapers.gsapubs.org on November 29, 2014

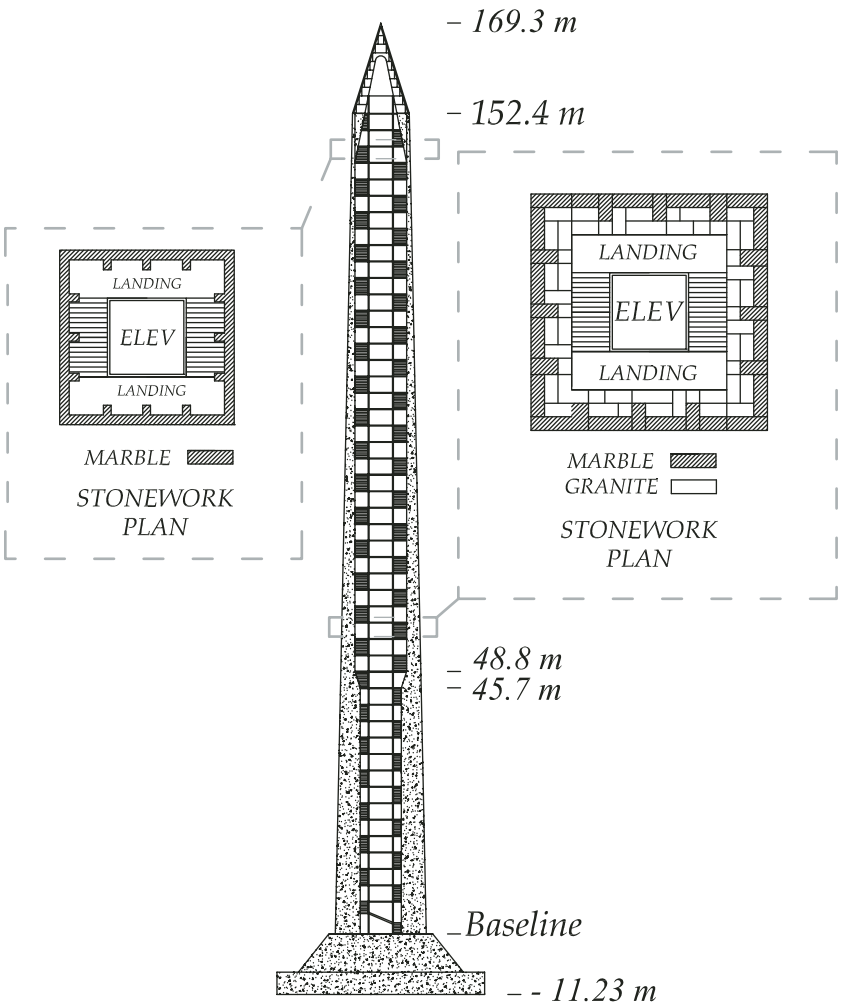

Figure 1. East elevation and section views of the Washington Monument.

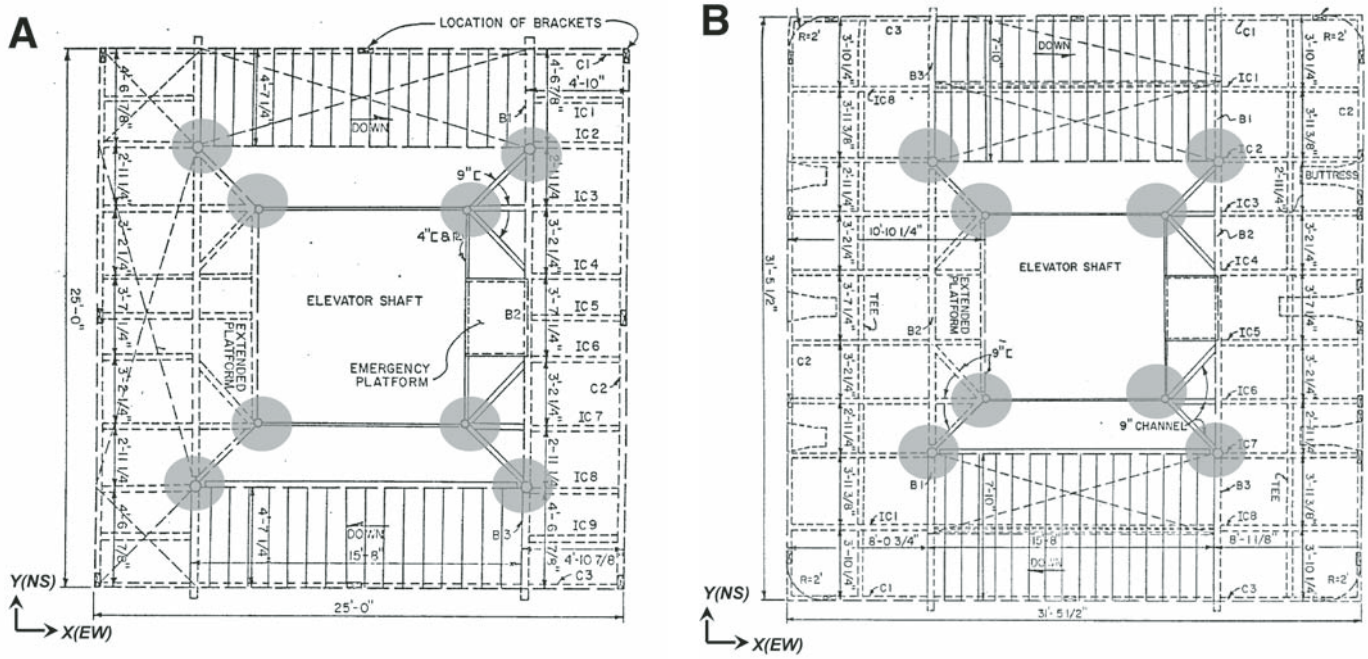

Figure 2. Detailed interior structure of the Washington Monument. (A) 150 ft (45.7 m) level and (B) 160 ft (48.8 m) level (Oehrlein and Associates Architects, 1993) Note: Gray circles represent vertical iron Phoenix columns and 25′ = 7.6 m and 31′-5 1/2″ = 9.6 m.

Downloaded from specialpapers.gsapubs.org on November 29, 2014

of the structure; these are Phoenix columns (an innovation of the Phoenix Iron Works, Phoenixville, Pennsylvania), each a circular pipe column made of iron, commonly used during the time of this construction.

POST-EARTHQUAKE ASSESSMENT OF THE WASHINGTON MONUMENT: OBSERVED DAMAGE

The WAMO was damaged during the 2011 Virginia earthquake, causing it to be closed to the public until repairs could be completed (May 2014). The main types of damage observed in the WAMO were cracking and spalling of the exterior stone. Cracking and spalling occurred over the entire height of the structure; a larger density of cracking occurred in the pyramidion as well as the upper section of the shaft around the 137.2 m level. Figure 3 shows examples of cracking in the marble pyramidion panels. The crack shown in Figure 3A is 1.32 m in length and 18 cm deep, and cuts through the entire depth of the marble panel. Figure 3B shows a close-up view of cracking of a previously repaired crack in a pyramidion panel.

Examples of the observed spalling are provided in Figure 4, including spalling of the corner of a marble pyramidion panel and a complex spall at a previously repaired corner.

Some of the observed damage had been documented in previously published historic assessment reports and did not necessarily occur during the 2011 Virginia earthquake. In order to investigate this issue, Figure 5 presents a timeline of the documented condition surveys of the WAMO. Figure 5A shows the condition of the exterior stones of the WAMO in 1934 (John Milner Associates, Inc., 2004); where the spalling was more severe below the 45.7 m level of the shaft. Figure 5B displays the results of a crack survey on the exterior of the WAMO published in 1993, which shows two main categories of cracking on all faces of the monument: (1) lower level cracks, between the 48.8 m and 71.3 m levels, and (2) the upper level cracks, above the 137.2 m level (Oehrlein and Associates Architects, 1993). Figures 5C and 5D respectively, show vertical cracking above the 45.7 m level (west elevation) and 128 m level (inside) the monument, documented in 2004 (John Milner Associates, Inc., 2004). Figures 5E–5G are from the post-earthquake assessment of the WAMO performed by Wiss, Janney, Elstner Associates, Inc. (2011), and show the loss of mortar in a vertical joint above the 137.2 m level, the cracking of a previously repaired vertical joint on the west elevation, and deep spalling on the west elevation near the pyramidion. Figure 5H, published in *The Washington Post* (9 July 2012), shows the damaged masonry stones of the WAMO on its four elevations. These observations from the timeline imply that the 2011 Virginia earthquake-induced damage on the WAMO is most likely on the pyramidion and upper and middle levels of the masonry shaft.

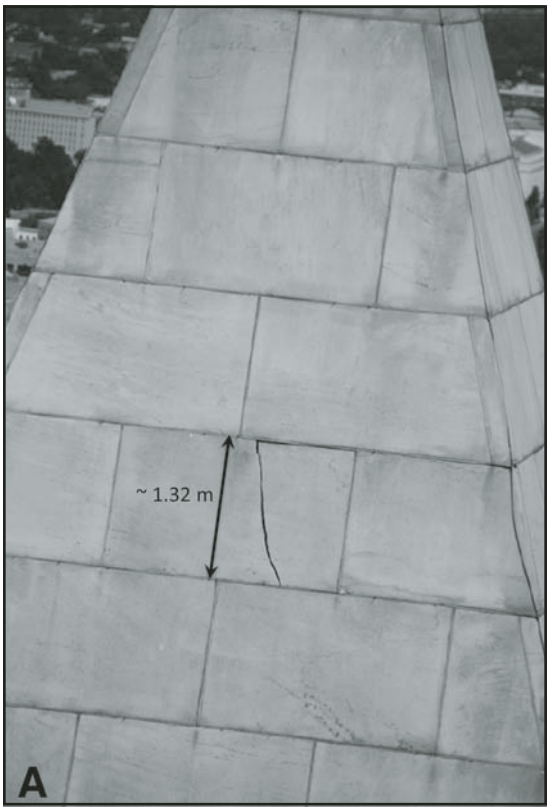

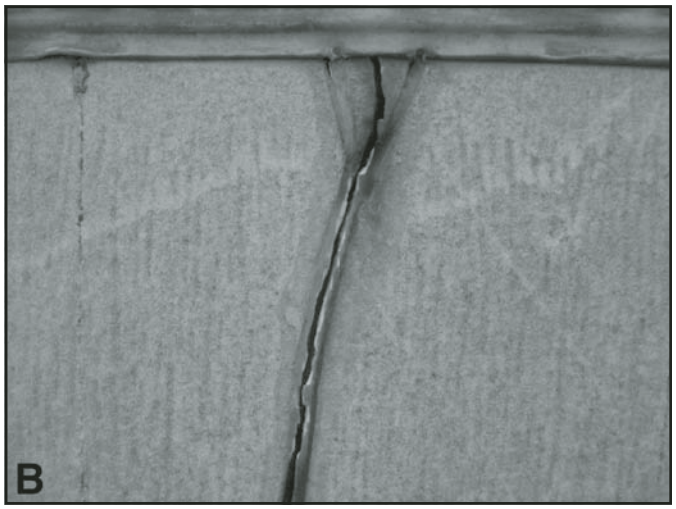

Figure 3. Cracking in pyramidion of the Washington Monument. (A) A newly developed crack on the west face of the pyramidion (B) Additional cracking along a historic crack (Wiss, Janney, Elstner Associates, Inc., 2011).

Downloaded from specialpapers.gsapubs.org on November 29, 2014

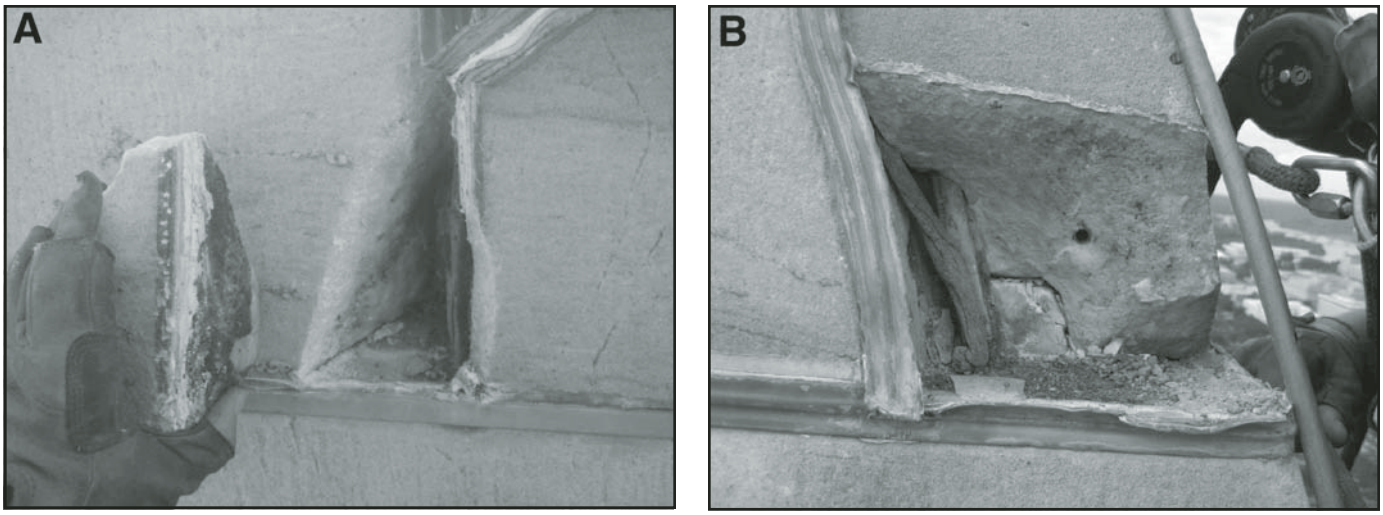

Figure 4. Spalling of pyramidion panels of the Washington Monument. (A) North face. (B) Northeast corner (Wiss, Janney, Elstner Associates, Inc., 2011).

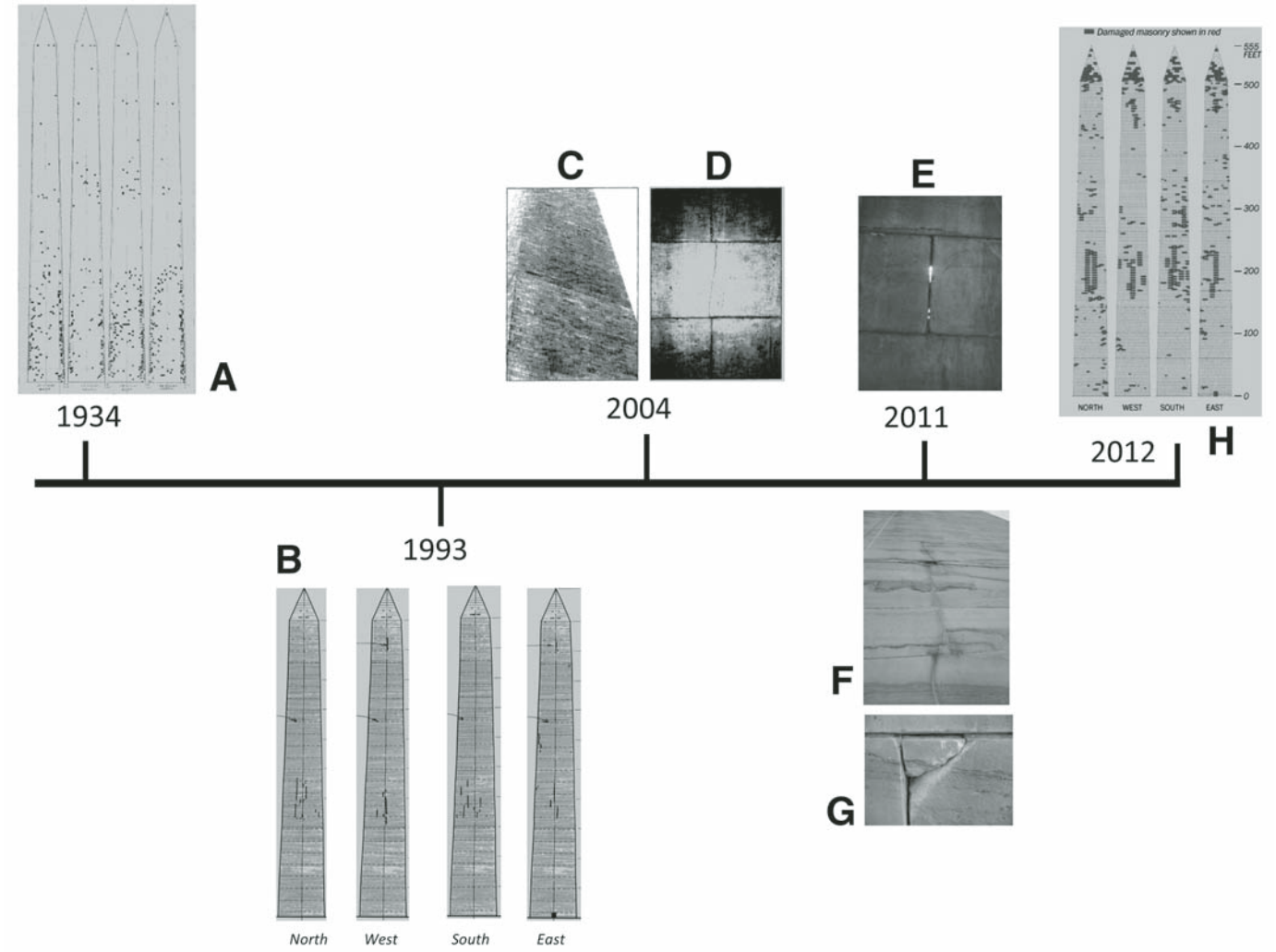

Figure 5. Timeline of the Washington Monument condition survey.

Downloaded from specialpapers.gsapubs.org on November 29, 2014

FINITE ELEMENT MODELING OF THE WASHINGTON MONUMENT

This section describes the procedure adopted in this study to create the FEM of the structure. In the analytical modeling of WAMO, like any other structural systems, a number of assumptions are made, particularly in terms of material properties. Hence, the calibration of the model with the vibration characteristics of the structure from field testing is essential prior to deriving any conclusions regarding the causes of the damage due the earthquake.

Model Properties

Information obtained from the blueprints of the WAMO was used to construct a three-dimensional (3D) FEM of the structure using the computer program SAP2000 (Computer and Structures, Inc., 2014, http://www.csiamerica.com/). The overall dimensions used for the exterior of the WAMO were a height of 152.4 m from the base to the bottom of the pyramidion with baseline dimensions of 16.9 m. The interior dimensions were 7.6 m by 7.6 m from the base up to the 45.7 m level, where they expand linearly to 9.6 m by 9.6 m at the 48.8 m level and continue up to the 152.4 m level. The wall thickness of the structure varied from 4.6 m at the base to 0.46 m at the top.

This study is primarily concerned with the modeling of the WAMO shaft, and thus the details of the pyramidion section were not included in the model. However, its effect was modeled as a distributed vertical gravity force at multiple locations from the 143.3 m level (where the panels that support the pyramidion are integrated into the shaft's walls) to the 152.4 m level, adding up to the estimated weight of the pyramidion. Choosing the dead load as the source to define the nodal masses for the dynamic analysis, the corresponding pyramidion mass was added to the nodal lumped masses obtained from the solid elements in the FEM.

As shown in Figure 1, the outer walls of the WAMO are constructed from a combination of marble and granite. Therefore, in the model, an average of the material properties of these two types of stone was used. Table 1 shows the range of values for the modulus of elasticity and unit weight of granite, marble, and iron; 45 GPa and 85 GPa were used as lower and upper bounds of the modulus of elasticity of the stone and 25.9 kN/m^3 for its unit weight. The material model for iron was defined using 190 GPa and 210 GPa as lower and upper bound values, and 76.2 kN/m^3 unit weight.

TABLE 1. MATERIAL PROPERTIES OF STONE AND IRON

Material	Elastic modulus (GPa)	Unit weight (kN/m^3)
granite	40–70	26.4
marble	50–100	25.1
iron	190–210	76.2

The FEM of the masonry shaft was constructed using 3D solid elements. In order to ensure the accuracy of the model, different meshes were developed by increasing the number of elements in each model (shown in Fig. 6). Among these, the FEM with 5600 solid elements (shown in Fig. 6D) was chosen since using a finer mesh of elements would change the natural frequencies of the model <0.1%. Phoenix columns were modeled with beam elements defined with pipe section properties. In order to include the effects of the stairs and platforms, diaphragm constraints are assigned to the inner nodes of the shaft at each 3.05 m level.

The foundation was modeled as a lumped mass located at its center of mass, and a group of uncoupled springs at the base of the foundation represents the compliance of the substructure with respect to translation and rotation about all three principal directions of the model. The stiffness of these springs was calculated according to the Federal Emergency Management Agency (FEMA) 356, *Prestandard and Commentary for Seismic Rehabilitation of Buildings* (FEMA 356, November 2000; https://law.resource.org/pub/us/code/bsc.ca.gov/sibr/gov.fema.fema356.pdf). In this method, the foundation is assumed rigid with respect to the supporting soil, and the uncoupled spring model represents the stiffness of the surrounding soil. The equivalent spring coefficients are found based on the dimensions of the footing and effective shear modulus of the underlying soil. In this procedure, values for the unit weight and Poisson ratio of the soil were respectively assumed as 17 kN/m^3 and 0.2, and the average measured shear wave velocity of 388.4 m/s of the soil strata to the base of foundation were used. Correction factors are applied in order to consider the effect of the soil embedment on the foundation stiffness. Table 2 summarizes the stiffness of the springs used to model the substructure.

PARAMETRIC STUDY OF STRUCTURAL AND GEOTECHNICAL MODELING UNCERTAINTIES

In order to consider the uncertainty associated with the adopted modeling approach, as well as the impact of foundation modeling, different cases were studied by permutation of the material properties of the structure as well as the stiffness of the foundation springs. The average of the lower and upper bounds of elastic modulus of granite and marble were used as the lower and upper bound values of the modulus of elasticity of the stone throughout the shaft. Therefore, the lower bound of the stone modulus of elasticity was assumed to be 45 GPa (average of 40 and 50 GPa), and a value of 85 GPa (average of 70 and 100 GPa) was used as the upper bound. The lower and upper bound values of the foundation stiffness were established using factors of 0.5 and 2 to the stiffness calculated based on FEMA 356 to account for the uncertainty associated with the modeling of the foundation. To this end, 12 different cases of FEMs were studied; the first 6 cases are based on estimated lower and upper bound values for material properties and foundation stiffness, and the last 6 cases are based on assumption of average elasticity moduli for stone and iron, and foundation stiffness having values shown in Table 2.

Downloaded from specialpapers.gsapubs.org on November 29, 2014

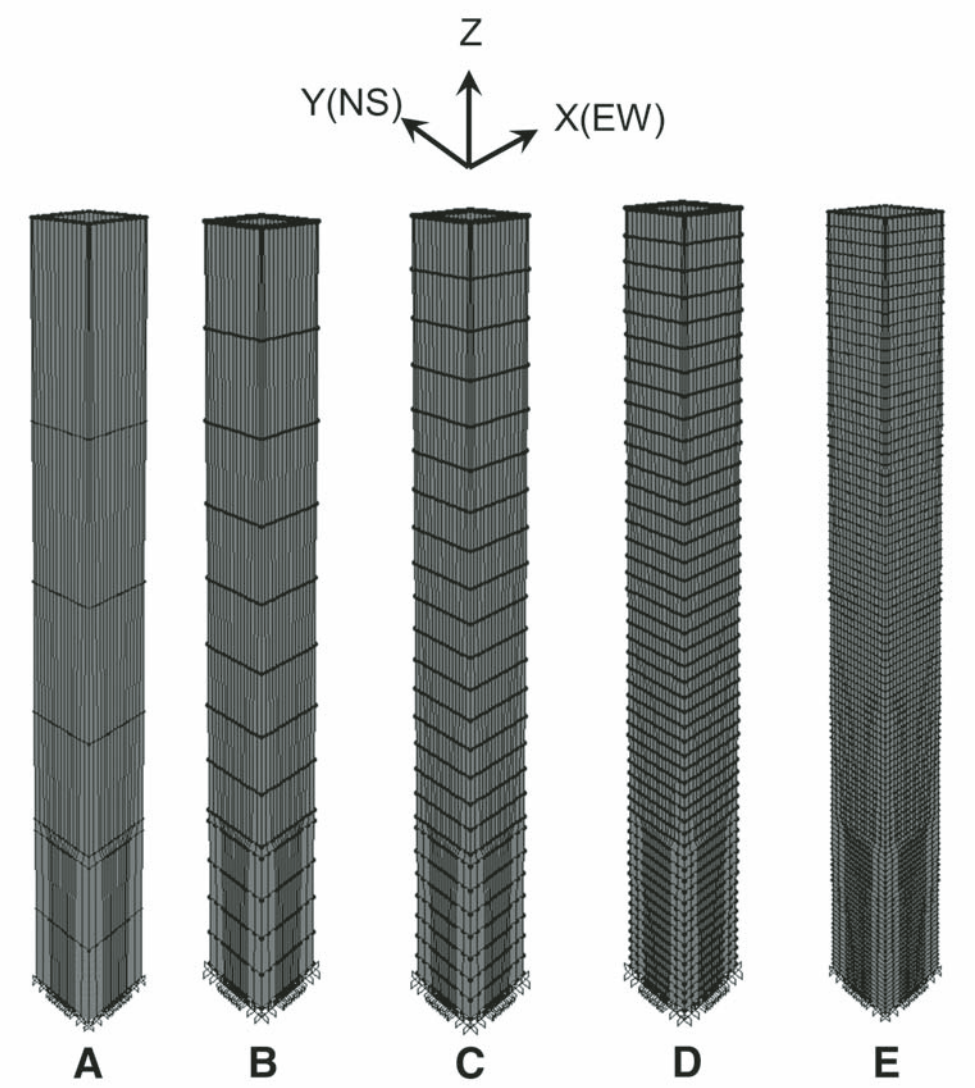

Figure 6. Finite element models of the Washington Monument masonry shaft. (A) 784 solid elements. (B) 1456 solid elements. (C) 2800 solid elements. (D) 5600 solid elements. (E) 11,200 solid elements.

In case 1, the modeling of the foundation is not considered, and the iron and stone in the superstructure were modeled using the upper bound value of the moduli of elasticity given in Table 1. In cases 2 and 3, upper and lower bound values of the foundation stiffness were considered, respectively, while the superstructure material properties are the same as that in case 1. Three other permutations are made by assigning the lower bound moduli of elasticity to the masonry shaft and the Phoenix columns to create cases 4–6. In case 4, the superstructure is modeled with the lower bound value of the material properties and is fixed at the ground level. In cases 5 and 6, the lower bound values for the material properties of the superstructure are used; however, the foundation is modeled with upper bound (case 5) and lower bound (case 6) values. Case 7 is created by assigning average of lower and upper bound values of the moduli of elasticity (65 GPa) to stone and iron without including the foundation in the model. In case 8, foundation springs (having the values shown in Table 2) are added to this model. Cases 9

TABLE 2. DESCRIPTION OF THE WASHINGTON MONUMENT FOUNDATION SPRINGS

Spring	Degree of freedom	Stiffness	Unit
KX	Translation along X-axis	4.2806E+07	
KY	Translation along Y-axis	4.2806E+07	kN/m
KZ	Translation along Z-axis	3.5268E+07	
KXX	Rocking about X-axis	1.2552E+10	
KYY	Rocking about Y-axis	1.2552E+10	kN.m/rad
KZZ	Torsion about Z-axis	2.6467E+10	

Downloaded from specialpapers.gsapubs.org on November 29, 2014

TABLE 3. DESCRIPTION OF THE PARAMETRIC STUDY

FEM*	Superstructure material properties	Substructure stiffness
Case 1	maximum moduli of elasticity	foundation was not modeled
Case 2	maximum moduli of elasticity	maximum estimated stiffness
Case 3	maximum moduli of elasticity	minimum estimated stiffness
Case 4	minimum moduli of elasticity	foundation was not modeled
Case 5	minimum moduli of elasticity	maximum estimated stiffness
Case 6	minimum moduli of elasticity	minimum estimated stiffness
Case 7	average moduli of elasticity	foundation was not modeled
Case 8	average moduli of elasticity	from Table 2
Case 9	average moduli of elasticity	maximum estimated stiffness
Case 10	average moduli of elasticity	minimum estimated stiffness
Case 11	maximum moduli of elasticity	from Table 2
Case 12	minimum moduli of elasticity	from Table 2

*Finite element models, Washington Monument (see text for explanation).

and 10 are created to study the effect of uncertainty in foundation stiffness when the superstructure is modeled with average of the bounds of the material properties. In cases 11 and 12, upper and lower values for the material properties of the superstructure are used, while foundation springs are modeled with values tabulated in Table 2. Table 3 summarizes the modeling assumptions of this parametric study.

Tables 4 and 5 present the results of modal analysis of these 12 cases. These tables show that the structural characteristics change extensively with the permutation of the material properties and the foundation stiffness. In addition, modeling the foundation significantly affects the period and shape of the structural vibration modes in the model.

Structural Identification through Ambient Vibration Measurements

The FEM of the WAMO is subjected to the 2011 Virginia earthquake record to simulate the behavior of the structure during this event and to investigate the causes of the observed damage, so it is essential to minimize the uncertainty in the finite element modeling results. As an attempt toward this end, field vibration tests were conducted to establish the dynamic characteristics of the structure and use them as a basis to select the FEM case that best represents the actual structure. This section presents the details of instrumentation, vibration monitoring, and structural identification of the WAMO.

TABLE 4. PERIODS OF VIBRATION AND DESCRIPTION OF THE MODE SHAPES, FEM CASES 1–6

Mode	Case 1		Case 2		Case 3		Case 4		Case 5		Case 6	
number	P	M.D.	P	M.D.	P	M.D.	P	M.D.	P	M.D.	P	M.D.
1	0.809	trans-Y	1.014	trans-Y	1.495	trans-Y	1.112	trans-Y	1.266	trans-Y	1.667	trans-Y
2	0.809	trans-X	1.014	trans-X	1.494	trans-X	1.112	trans-X	1.265	trans-X	1.667	trans-X
3	0.218	trans-Y	0.288	trans-Y	0.414	axial	0.300	trans-Y	0.359	trans-Y	0.451	trans-Y
4	0.218	trans-X	0.288	trans-X	0.372	trans-Y	0.300	trans-X	0.359	trans-X	0.451	trans-X
5	0.116	torsional	0.211	axial	0.372	trans-X	0.159	torsional	0.217	axial	0.417	axial
6	0.099	trans-Y	0.146	trans-Y	0.216	trans-Y	0.136	trans-Y	0.175	trans-Y	0.246	trans-Y
7	0.099	trans-X	0.146	trans-X	0.216	trans-X	0.136	trans-X	0.175	trans-X	0.246	trans-X
8	0.073	axial	0.120	torsional	0.134	torsional	0.100	axial	0.162	torsional	0.172	torsional
9	0.058	trans-Y	0.097	trans-Y	0.114	trans-Y	0.080	trans-Y	0.117	trans-Y	0.148	trans-Y
10	0.058	trans-X	0.097	trans-X	0.114	trans-X	0.080	trans-X	0.117	trans-X	0.148	trans-X

Note: FEM—finite element model (see text). P—period (s). M.D.—mode description (trans—translational).

TABLE 5. PERIODS OF VIBRATION AND DESCRIPTION OF THE MODE SHAPES, FEM CASES 7–12

Mode	Case 7		Case 8		Case 9		Case 10		Case 11		Case 12	
number	P	M.D.	P	M.D.	P	M.D.	P	M.D.	P	M.D.	P	M.D.
1	0.925	trans-Y	1.272	trans-Y	1.107	trans-Y	1.556	trans-Y	1.193	trans-Y	1.409	trans-Y
2	0.925	trans-X	1.271	trans-X	1.107	trans-X	1.556	trans-X	1.193	trans-X	1.409	trans-X
3	0.250	trans-Y	0.354	trans-Y	0.315	trans-Y	0.415	axial	0.324	trans-Y	0.399	trans-Y
4	0.250	trans-X	0.354	trans-X	0.315	trans-X	0.402	trans-Y	0.324	trans-X	0.399	trans-X
5	0.132	torsional	0.296	axial	0.213	axial	0.402	trans-X	0.295	axial	0.298	axial
6	0.113	trans-Y	0.187	trans-Y	0.157	trans-Y	0.229	trans-Y	0.176	trans-Y	0.203	trans-Y
7	0.113	trans-X	0.187	trans-X	0.157	trans-X	0.229	trans-X	0.176	trans-X	0.203	trans-X
8	0.083	axial	0.140	torsional	0.136	torsional	0.148	torsional	0.125	torsional	0.165	torsional
9	0.067	trans-Y	0.118	trans-Y	0.105	trans-Y	0.128	trans-Y	0.107	trans-Y	0.134	trans-Y
10	0.067	trans-X	0.118	trans-X	0.105	trans-X	0.128	trans-X	0.107	trans-X	0.134	trans-X

Note: FEM—finite element model (see text). P—period (s). M.D.—mode description (trans—translational).

Downloaded from specialpapers.gsapubs.org on November 29, 2014

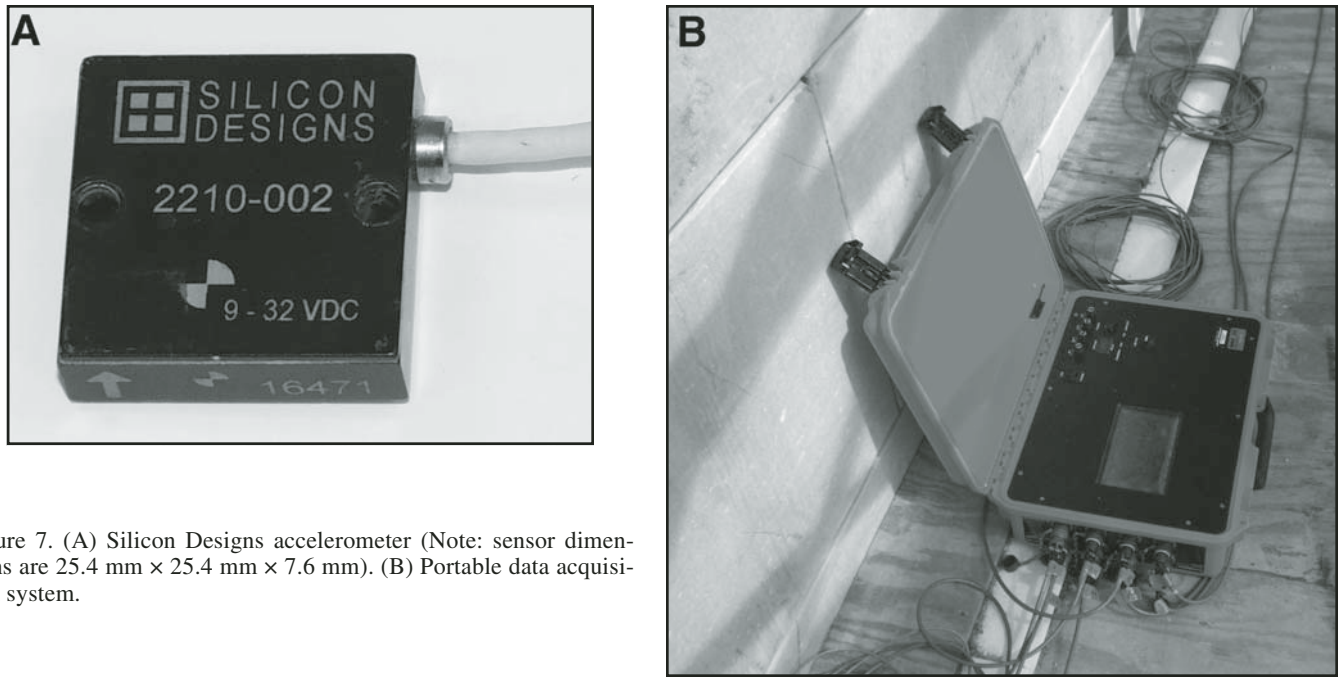

Figure 7. (A) Silicon Designs accelerometer (Note: sensor dimensions are 25.4 mm × 25.4 mm × 7.6 mm). (B) Portable data acquisition system.

Ambient vibration measurement of the WAMO was conducted using a network of eight sensors and a portable data acquisition system (shown in Fig. 7). The sensors are single-channel accelerometers manufactured by Silicon Designs, Inc. (model 2210–002; http://www.silicondesigns.com/ds/ds2210.html). The data acquisition system has a 24-bit analog to digital convertor, with a quantization resolution of <1 μg. The sensors have a characteristic noise floor of 13 μg√Hz, which for a signal filtered at 15 Hz translates to ~50 μg root mean squared (RMS) noise.

Two wired accelerometers were located at each corner of the masonry shaft of the WAMO at the 149.7 m level to measure the horizontal vibration of the structure in two orthogonal transverse directions. Figure 8 shows the layout of this sensor network and Figure 9 shows sensors A1, A2, A3 and A4 attached to the monument. Ambient vibrations were measured for over a 60 min duration using a sampling frequency of 200 Hz (720,000 samples/channel).

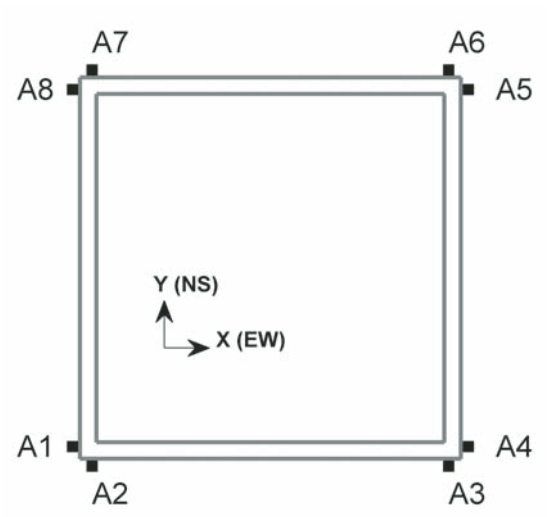

Figure 8. Layout of deployed sensor network (A1–A8; level 149.7 m).

Figure 10 shows the time history of the data collected at the southwest corner of the WAMO after removing the unwanted trend due to temperature change caused by wind and sunshine. This figure shows that the ambient vibration amplitude is ~300 μg. The collected data are further studied in the frequency domain. Figure 11 presents the average power spectral density of the eight measured signals obtained using the Welch (1967) method. This figure shows distinct peaks of the power spectral density, corresponding to the natural vibration frequencies of the system. The peaks are distinct and clear, and repeat in data from all sensors.

Modal Parameter Identification

Modal parameter identification is performed using the output-only Eigen realization algorithm. Using a software package developed at Lehigh University (Bethlehem, Pennsylvania) for convenient modal identification of dynamic systems (SMIT; Structural Modal Identification Toolsuite; Chang and Pakzad, 2013), the optimum model order was found from the stabilization diagrams [with convergence thresholds of 5%, 95%, and 10% for frequencies, modal assurance criterion (MAC) values (Allemang, 2003), and damping ratios, respectively] and the modal properties were extracted. Figure 12 shows the stabilization diagrams created based on the ambient acceleration signals measured in

Downloaded from specialpapers.gsapubs.org on November 29, 2014

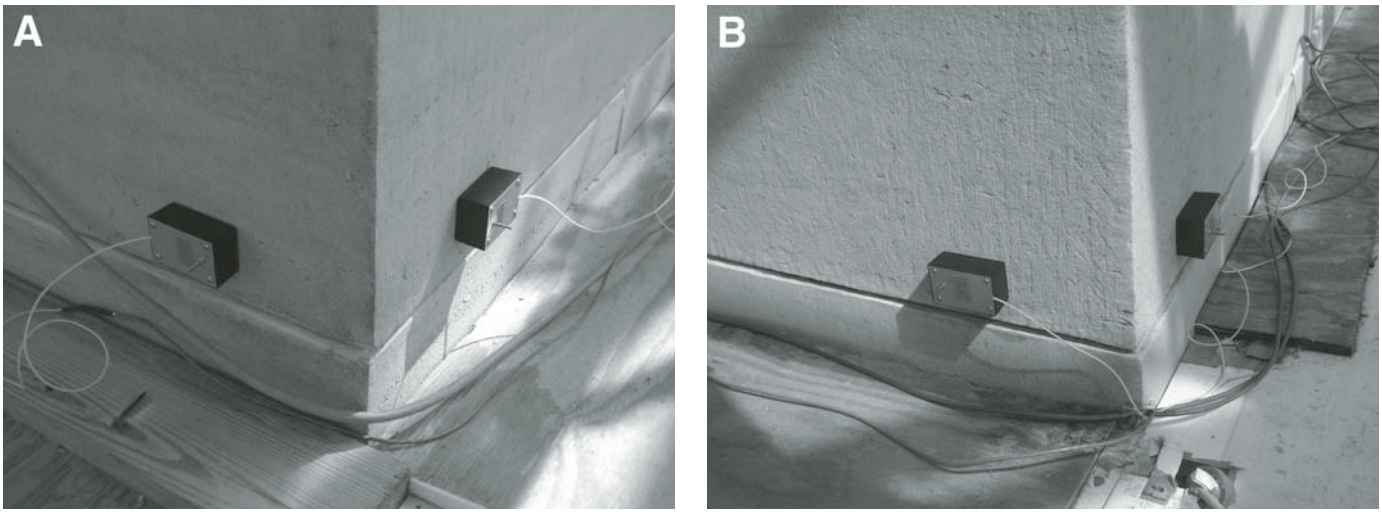

Figure 9. Single channel wired sensors A1 through A4 at 491 ft. (149.7 m) level; (A) A1 and A2 located at south-west corner, (B) A3-A4 located at south-east corner.

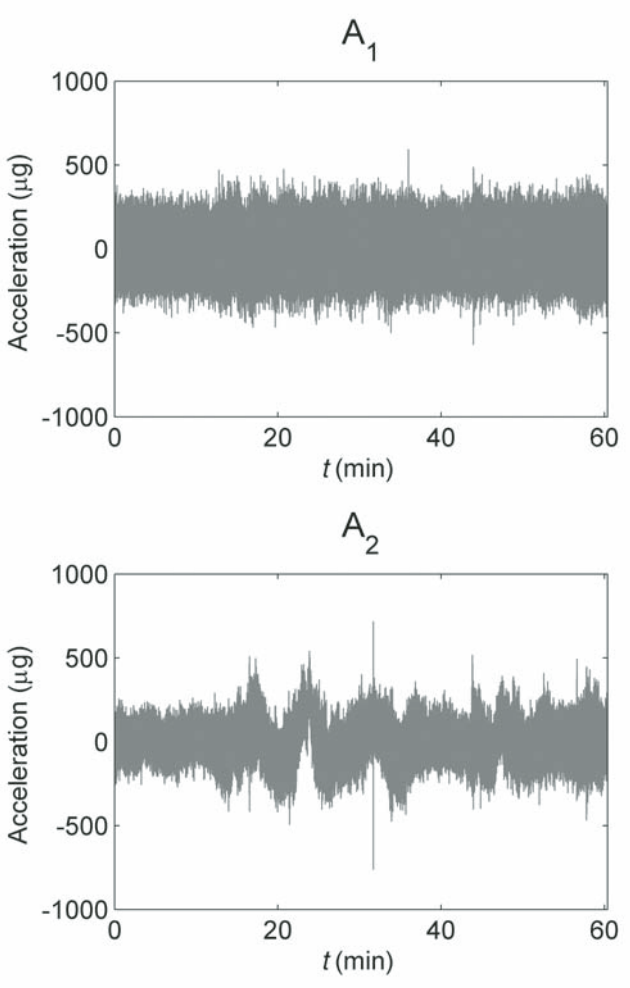

Figure 10. Collected data through sensors A1 and A2 (after detrending); *t* is time.

the east-west and north-south directions. In these plots, the identified modal parameters at every model order are marked if they fall within the prespecified stability threshold of the identified modal parameters at the previous model order.

Figure 13 shows the first seven identified structural modes using the entire data set. Because the sensor deployment was located at only one level of the WAMO, no spatial information along the height of the structure for the mode shapes is available, and thus the modal ordinates are used to distinguish between modes in the two transverse directions and twisting (i.e., torsional modes). Moreover, since in this project a short-term ambient vibration analysis was conducted, a study of the effect of environmental factors on the dynamic characteristics of the WAMO was not of primary focus.

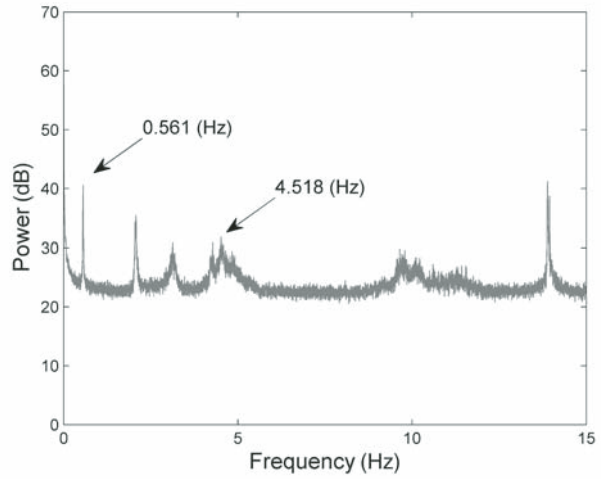

Figure 11. Average power spectral density of the collected data.

Downloaded from specialpapers.gsapubs.org on November 29, 2014

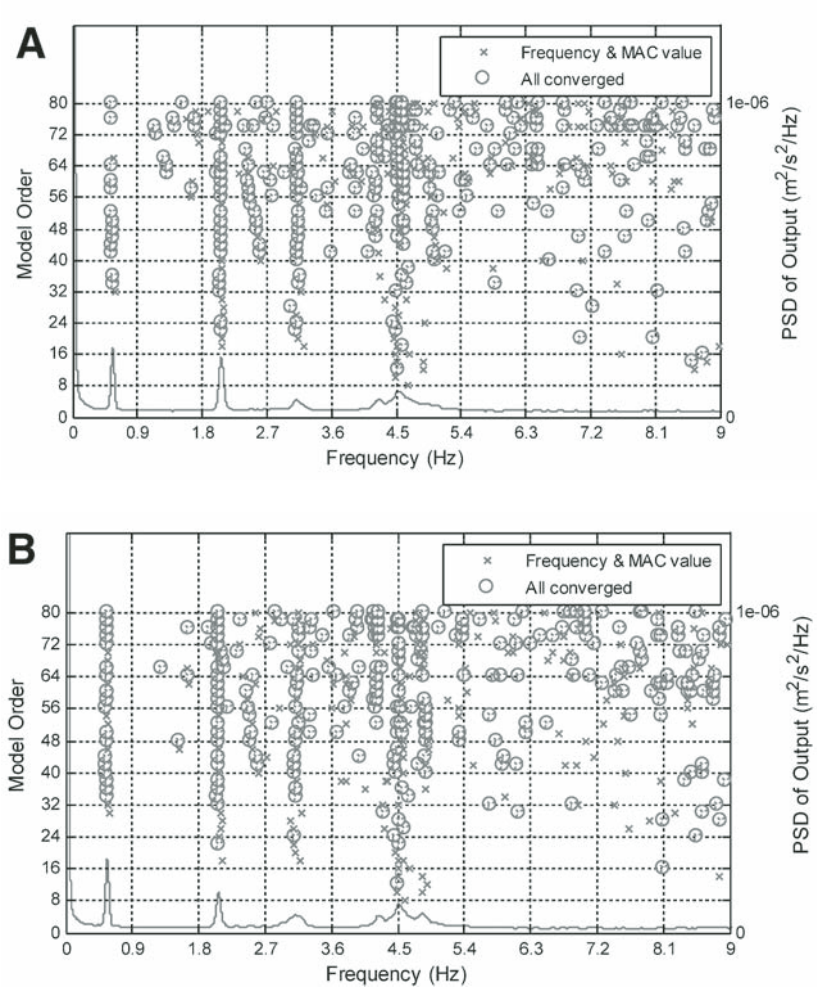

Figure 12. Stabilization diagrams in 0–9 Hz frequency range based on the acceleration signals. PSD—power spectral density; MAC—modal assurance criterion. (A) Measured in east-west (X) direction. (B) Measured in north-south (Y) direction.

VERIFICATION OF FEM USING IDENTIFIED MODAL QUANTITIES

A comparison of the identified natural periods of the structure and fundamental period of the finite element models shows that among all the cases studied before, the FEM in case 6 best represents the measured dynamic characteristics of the WAMO. In this case, the foundation is included in the FEM, and the lower bound values for the material properties of the superstructure and the stiffness of the substructure are used. Figure 14 illustrates four analytically identified vibrational modes of the structure in case 6: first-three translational modes in the Y-direction, along with the 8th mode (torsional deformation). Translational modes in the X-direction are not pictured here; in these modes the structure

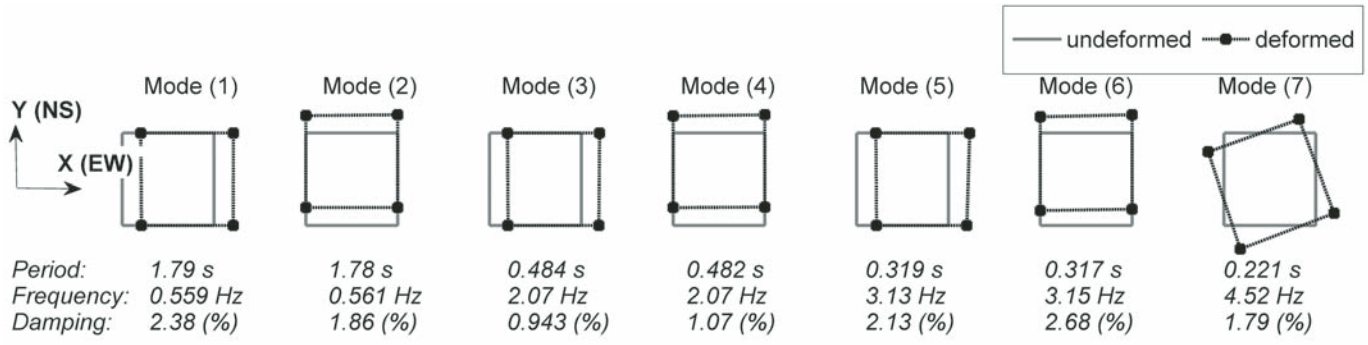

Figure 13. Experimentally identified structural modes, cross section of the Washington Monument at 149.7 m level.

Downloaded from specialpapers.gsapubs.org on November 29, 2014

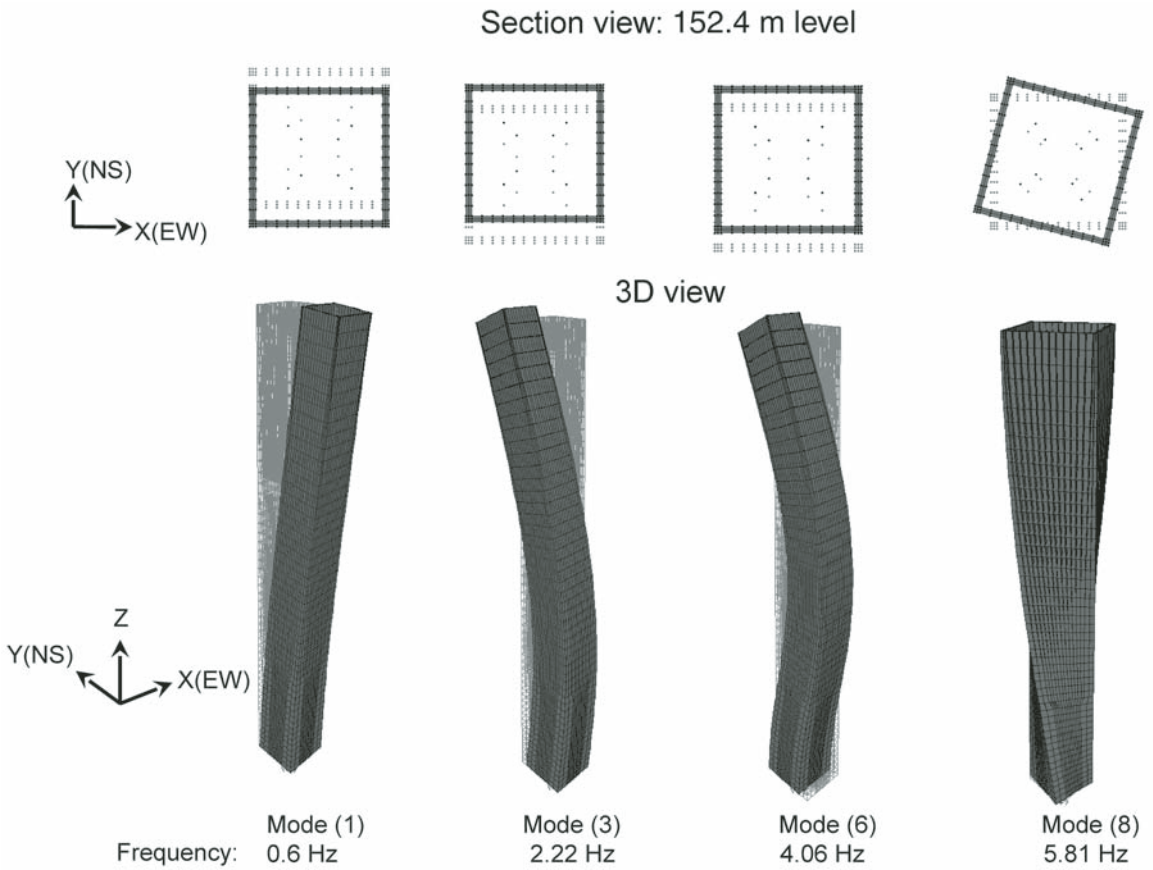

Figure 14. Analytical structural modes (case 6; see text). 3D—three dimensional.

vibrates at the same frequency and similar shape as those shown in Figure 14, but in the X-direction.

ESTIMATED GROUND SHAKING AT THE WAMO SITE

There were not any ground-motion recordings in the immediate Washington, D.C., area during the 2011 earthquake. In this study, the ground shaking at the WAMO site is estimated based on the ground-motion recording at Reston, Virginia, the station closest to Washington, D.C. As seen in Figure 15, the Reston recording station is located relatively close to the WAMO site, ~31 km away. The Reston recording station and WAMO sites are ~122 km and 131 km, respectively, from the earthquake epicenter. Site response analyses were performed using the recorded ground motion from Reston and the shear-wave velocity profiles at the station and WAMO sites as measured by the USGS. ProShake (EduPro Civil Systems, 2003, http://www.proshake.com), a 1D equivalent linear ground response analysis software, was used for this analysis. Relative orientations of the recording station site and the WAMO site with respect to the earthquake epicenter were considered in the angular transformation of the recorded and calculated motions.

The shear-wave velocity (Vs) profile at the Reston recording station site is shown in Figure 16. Rock with Vs = 2600 m/s is encountered at a relatively shallow depth at this site; located at a depth of 42 m. The bidirectional (east-west and north-south) ground motions recorded at the Reston station were rotated into

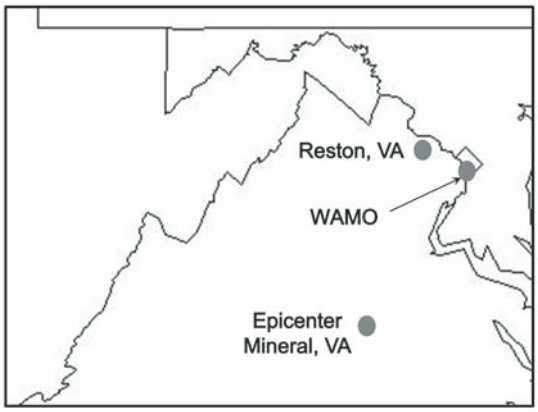

Figure 15. Location map showing the earthquake epicenter, Reston (VA—Virginia) recording station, and the Washington Monument (WAMO).

Downloaded from specialpapers.gsapubs.org on November 29, 2014

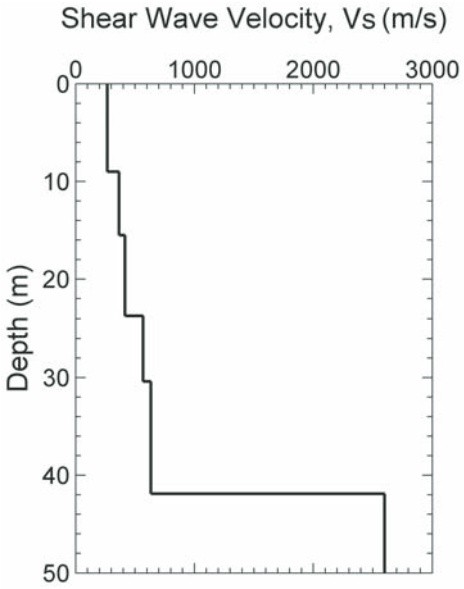

Figure 16. Shear-wave velocity (Vs) profile at Reston, Virginia, recording station.

path-parallel and path-normal components along the source-to-recording site orientation (Mineral-Reston). These components at the ground surface were then deconvoluted to hard rock level (Vs = 3500 m/s) at Reston using the Vs profile at the station site. For Reston, it was assumed that this Vs = 3500 m/s material corresponding to the hard rock motions was located at a depth of 550 m with a transition from 42 m depth.

Hard rock motions in Reston can be considered to be representative of the hard rock motions at the WAMO site due to their proximity and respective distances to the earthquake source. Hard rock motions at the base of the Reston profile were rotated into (Mineral-WAMO site) path-parallel and path-normal components. Site response analyses were performed using the rotated rock motions and these were then propagated up to the ground surface level at the WAMO site using the velocity profile at the site. Shear-wave velocity measurements by the USGS at WAMO extend to a depth of ~100 m below the ground surface, and these measurements are indicative of weathered rock with Vs ~1000 m/s. These observations are in agreement with other available information about the local geology and depth to rock (Darton, 1951). Since the hard rock underneath the WAMO is located below the deepest level of Vs profile measurements, there was the need to introduce reasonable assumptions for the conditions of hard rock at deeper levels. Two different profile scenarios were considered for the Vs profile beyond the extent of the measurements at WAMO, as shown in Figure 17. In one of these cases the measured Vs profile was directly augmented on top of hard rock with Vs = 2600 m/s, whereas the second profile included a 3-step transition from the base of the measurements to Vs = 2600 m/s material. For both cases, a smooth transition to Vs = 3500 m/s hard rock over 100 m was assumed below the Vs = 2600 m/s material. Site response analyses were performed for both cases to estimate the ground motions at the WAMO site during the 2011 Virginia earthquake. The ground motions resulting from the two profile scenarios are shown in Figure 18. The peak ground accelerations (PGA) of these motions are 0.054 g and 0.059 g in path-parallel and path-normal directions (Mineral-WAMO).

Angular transformation was used to rotate the estimated ground surface motions into east-west and north-south directions to be applied to the FEM of the system at the foundation level. Figure 19 shows these ground motions, which have 0.078 g and 0.042 g PGA, in east-west and north-south directions, respectively.

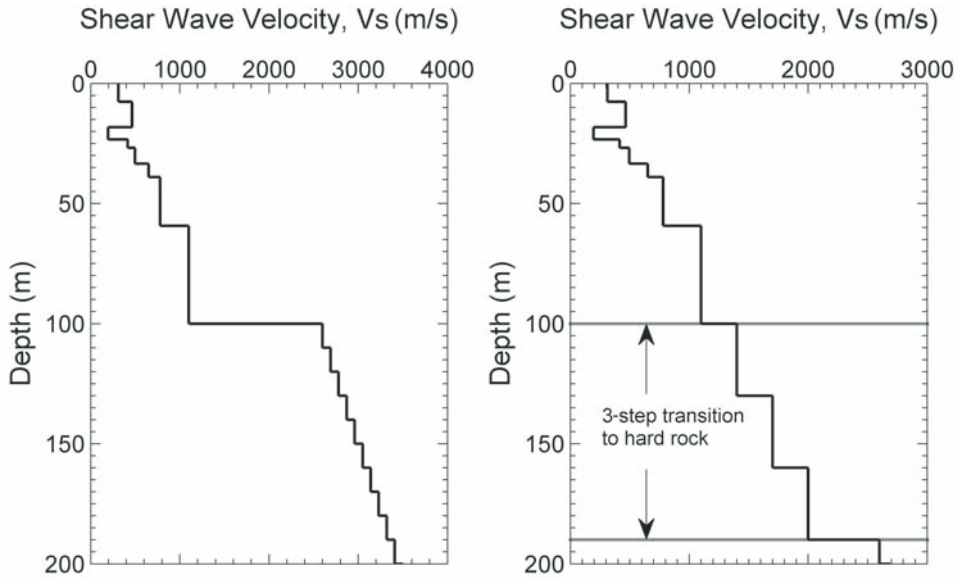

Figure 17. Shear-wave velocity (Vs) profile at the Washington Monument site used in the ground-motion response analyses considering two different transition scenarios for deeper rock levels. (A) No transition. (B) Three-step transition.

Downloaded from specialpapers.gsapubs.org on November 29, 2014

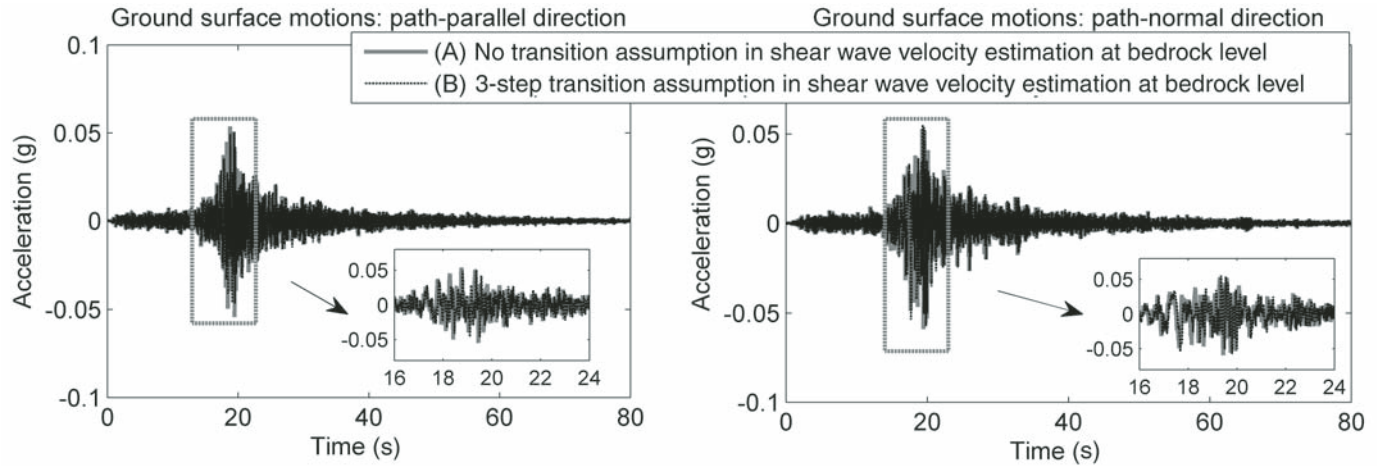

Figure 18. Estimated ground motions at the Washington Monument site during the Virginia earthquake (path-parallel and path-normal components).

RESPONSE SPECTRUM STUDY

Here we present the response spectrum analyses conducted on the estimated surface ground motions. Figure 20 show the 2% damped linear response spectra for the east-west and north-south directions of the ground shaking at the WAMO site (in terms of the pseudo-spectral acceleration), along with the FEM and measured ambient structural vibration periods. Figure 20 shows that the spectrum amplitudes (for both the east-west and north-south directions) of the records generated as scenarios A and B at the natural frequencies of the structure are close in pseudo-spectral acceleration value. In addition, the response amplitude at the first and second mode periods (1.79 s) is small, while the higher modes (modes 3, 4, 5, and 6) are in a region of larger spectral acceleration amplitude. Because contribution of each vibrational mode in the seismic performance of the structure also depends on the modal participation ratios, the mass participation of vibration models of the FEM in case 6 are reviewed in Table 6. This table shows that for the Washington Monument, a tall structure with nonuniform mass and stiffness distribution along its height, higher modes (the 2nd and 3rd translational modes in the horizontal X- and Y-directions, which are modes 3, 4, 6, and 7 of the structure) have large mass participation ratios. Large spectral amplification combined with high participation ratios imply that the higher structural modes have a greater dynamic amplification than the fundamental modes during the earthquake, and potentially a substantial contribution to the internal forces that developed in the structure.

TIME-HISTORY ANALYSIS RESULTS: PREDICTED DAMAGE

Time histories of the ground acceleration in the east-west and north-south directions were defined and applied

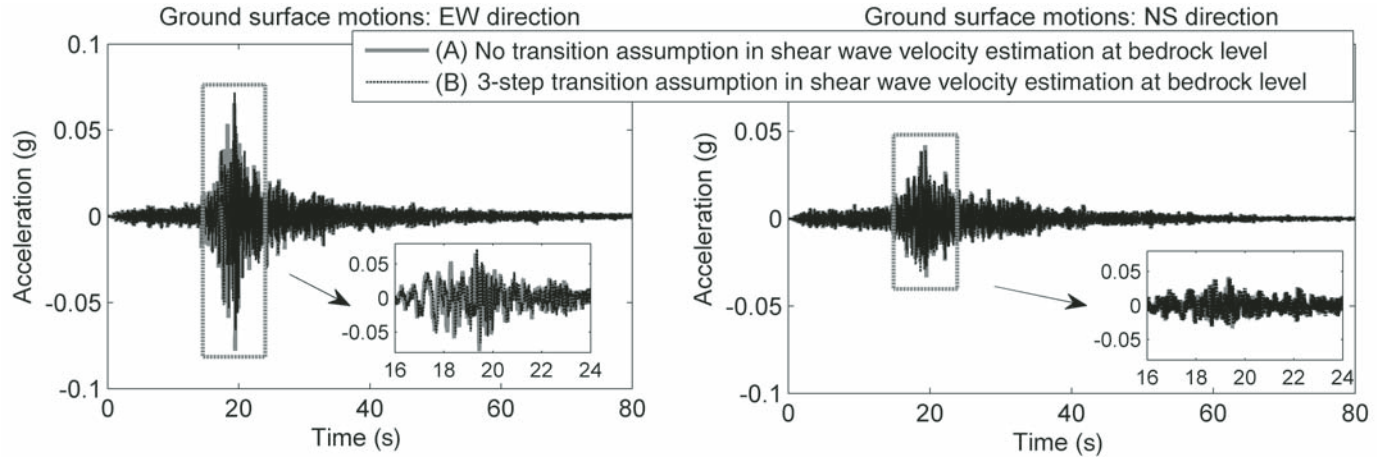

Figure 19. Estimated ground motions at the Washington Monument site during the Virginia earthquake (EW, NS—east-west and north-south components).

Downloaded from specialpapers.gsapubs.org on November 29, 2014

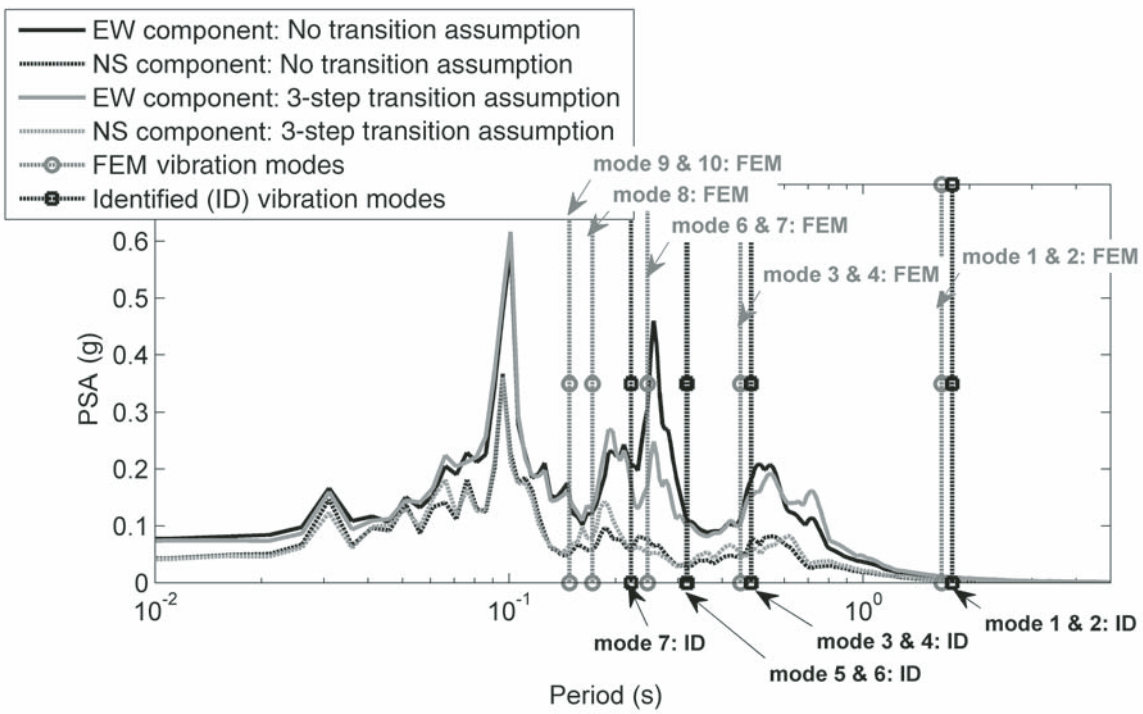

Figure 20. Linear response spectra of the east-west and north-south (EW, NS) components of the Virginia earthquake estimated at the Washington Monument site. FEM—finite element model; PSA—pseudo-spectral acceleration (see text).

bidirectionally to the base of the calibrated FEM in case 6. Linear modal time-history analyses were performed using a time step of 0.005 s and zero initial conditions. In this analysis, a damping ratio of 2% was used for the structure, in the range of the damping ratios obtained through the structural identification we undertook (shown in Fig. 13), and consistent with the identified damping ratios of masonry structures reported in the literature (De Sortis et al., 2005; Gentile and Saisi, 2007). Figure 21 shows the time histories of displacement and acceleration during the ground shaking at the observation level (152.4 m) of the WAMO, along with their peak values. Due to the structural characteristics of the Washington Monument, the acceleration at observation level is amplified by more than 8 and 5 times compared to the accelerations at the ground level in east-west and north-south directions, respectively. This high level of acceleration amplification can lead to the observed damage at the upper sections of the shaft, pyramidion, and fallen debris at the observation level. Figure 22 illustrates the distribution of the maximum tensile stresses (in the vertical Z-direction) on the outer surface due to the combined effect of the structure's weight and bidirectional ground motions over the entire history of the earthquake record. The color scale on the bottom of Figure 22 indicates the magnitude of the stresses; the highest tensile stresses are shown in dark gray and white represents zero tensile stress. The tensile stresses show a high concentration around the 107 m level. However, these tensile stresses are significantly smaller than the reported tensile strength of masonry stone. Based on the ASTM (formerly the American Society for Testing and Materials) specifications (Standards C503/C503M-10 and C615/C615M-11; ASTM, 2010a, 2011) moduli of rupture of marble and granite are 6.9 MPa and 10.3 MPa, respectively. Maximum compressive stress throughout the structure (−3.69 MPa) is also considerably smaller than the reported compressive strength of marble (−52 MPa), granite (−131 MPa), and grout (−13.8 MPa). Compressive strength of the grout was estimated based on ASTM specifications (Standard C476–10; ASTM, 2010b), and tensile strength of the grout was assumed to be ~10% of its compressive strength. Therefore, the concentration of the maximum tensile stresses (as shown in Fig. 22) could explain the cracking

TABLE 6. FEM MODAL PARTICIPATION RATIOS: CASE 6

Mode number	Period (s)	Mode description	Mass participation ratio	
			X (EW) direction	Y (NS) direction
1	1.667	trans-Y	0.00	0.40
2	1.667	trans-X	0.40	0.00
3	0.451	trans-Y	0.00	0.33
4	0.451	trans-X	0.33	0.00
5	0.417	axial	0.00	0.00
6	0.246	trans-Y	0.00	0.25
7	0.246	trans-X	0.25	0.00
8	0.172	torsional	0.00	0.00
9	0.148	trans-Y	0.00	0.02
10	0.148	trans-X	0.02	0.00

Note: FEM—finite element model (see text); trans—translational; EW—east-west; NS—north-south.

Downloaded from specialpapers.gsapubs.org on November 29, 2014

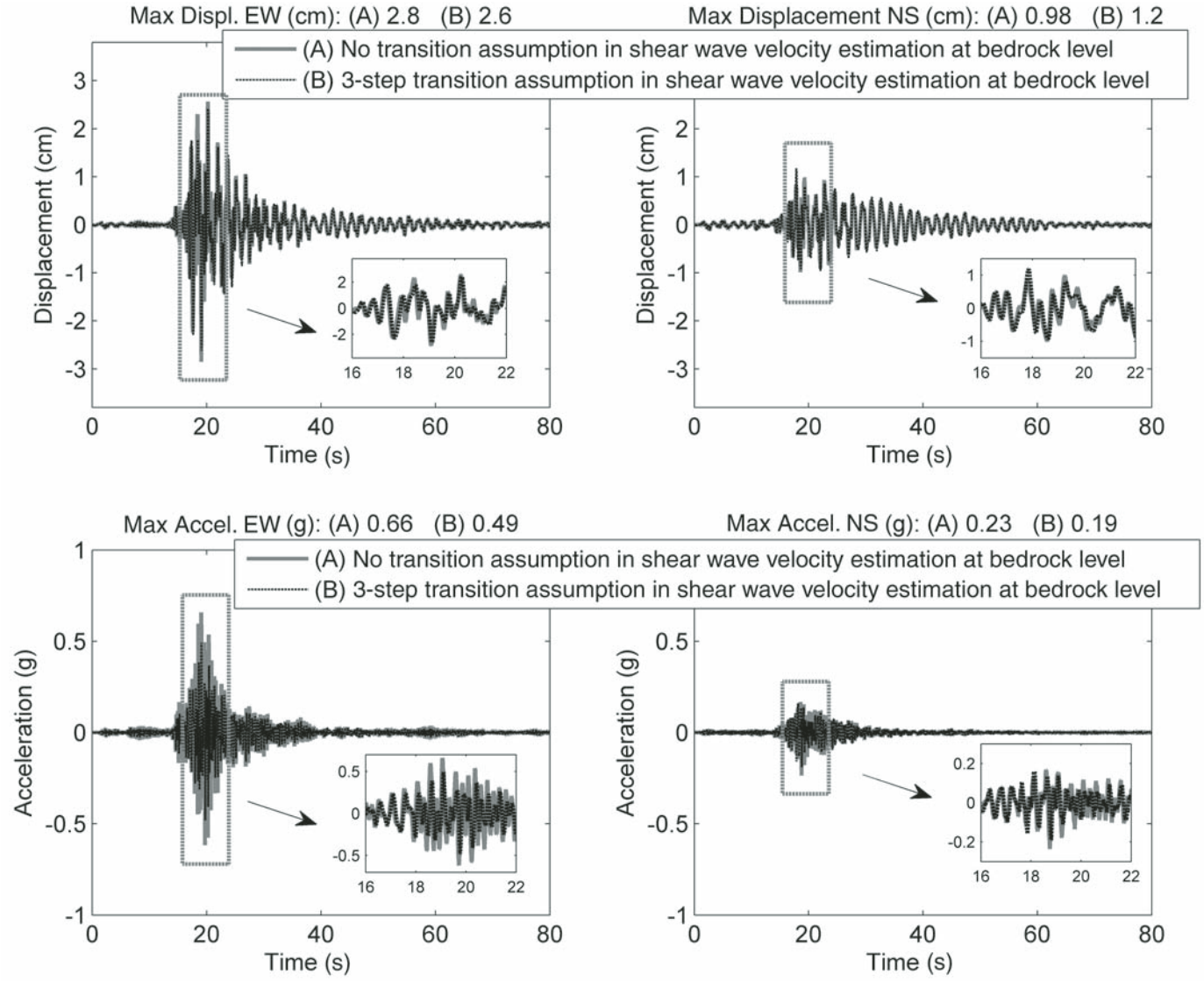

Figure 21. Structural response of the Washington Monument at 152.4 m level. Max Displ.—maximum displacement; Max Accel.—maximum acceleration; EW, NS—east-west, north-south.

damage at this location of the masonry shaft of the WAMO in terms of the mortar loss and recracking observed in the previously repaired cracks.

SUMMARY AND CONCLUSIONS

We investigated the potential causes of the damage to the WAMO sustained from the 2011 Virginia earthquake. For this purpose, an FEM of the superstructure was constructed based on the published historic blueprints. In this modeling, the details of the pyramidion were not included; instead its estimated weight was distributed on the upper levels of the masonry shaft. This method was adopted because the pyramidion is a significantly complex system, the modeling of which requires more information than available to the public. In addition, structural identification of the pyramidion requires access to the inside of the structure for sensor deployment, which was not feasible during this research. The foundation was modeled as a lumped mass located at its center of mass and a group of uncoupled springs at the base of the foundation to represent the compliance of the substructure.

In order to address the uncertainties regarding the material properties of the stone and iron of the superstructure and stiffness coefficients of the foundation in the absence of in situ material testing, a parametric study is completed where the parameters of the analytical model are permuted at different values to bound the predicted dynamic characteristics of the structure. To minimize such modeling uncertainty, preliminary ambient vibration tests were conducted to identify the modal properties of the structure.

Downloaded from specialpapers.gsapubs.org on November 29, 2014

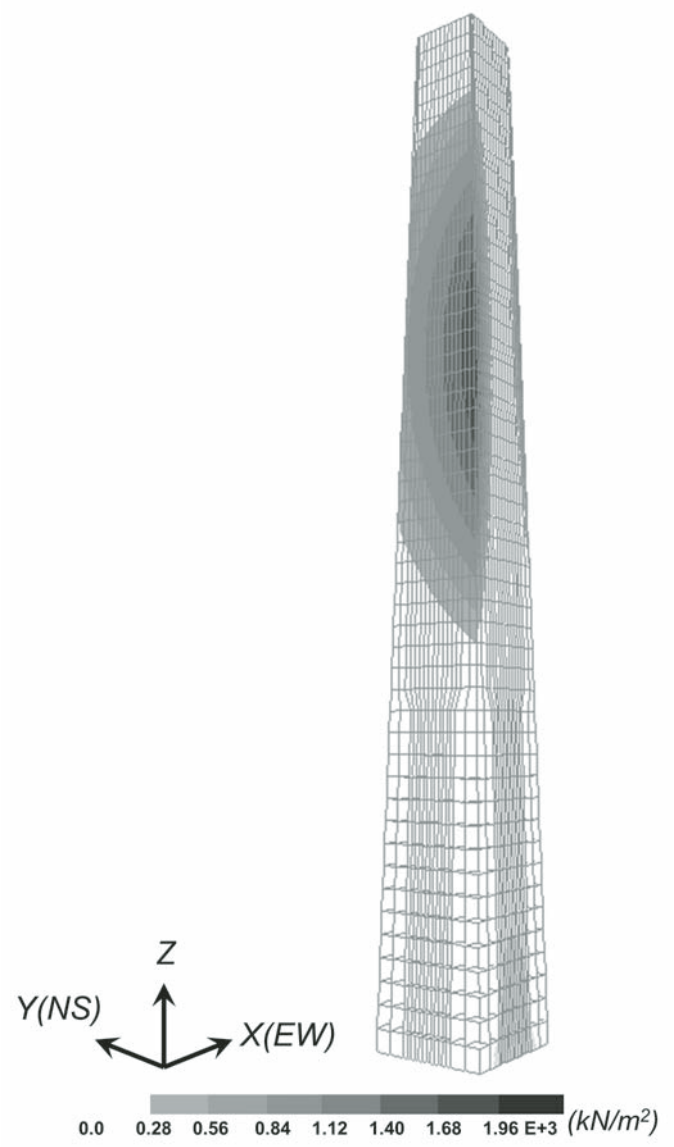

Figure 22. Envelope of the maximum tensile stresses in the vertical direction, Washington Monument. No transition assumed in shear-wave velocity estimation. EW, NS—east-west, north-south.

On the basis of these measured vibration modes, a set of model parameters (from the parametric study) was selected for further investigation. Due to the lack of ground shaking measurements in the Washington, D.C., area during the 2011 Virginia earthquake, the ground motions at the WAMO site were estimated using angular transformation of the deconvoluted ground motions in Reston, Virginia, to the bedrock level and upward propagation of the rotated motions to the ground surface based on the soil profiles in Reston and the WAMO site provided by USGS. The selected FEM of this structure was then subjected to the bidirectional ground motions and response of the model in terms of displacement, acceleration, and stress distribution. The following is a summary of the findings of this study.

- The parametric study in this research underlined the impact of modeling the foundation to make the analytical model a better representation of the actual structure. The bidirectional time-history analysis of the calibrated model revealed a large amplification of the acceleration at the observation level, along with concentration of the tensile stresses above the mid-height of the structure. These observations correlate with the observed damage in the WAMO caused by the 2011 Virginia earthquake.
- One purpose of this study was to investigate the effect of substructure flexibility on the modal properties of the FEM of the monument. For this purpose, a simplified soil-structure interaction analysis (based on FEMA 356) was adopted to perform a parametric study using different assumptions in the modeling of the substructure and superstructure. In the time-history analysis, the free field motions were used mainly because those motions were available to us. Also, three cases considered in the finite element modeling do not include the foundation in the FEM. A more sophisticated soil-structure interaction analysis consisting of modeling the soil strata beneath the structure may reveal more information.
- This study highlights the role that nondestructive structural identification tests play in decreasing the uncertainty associated with the analytical modeling of existing structures. Such experimentally calibrated structural models are beneficial in several applications, including identification of causes of structural damage, assessment of repair and retrofit alternatives, and predicting the behavior of the structure in future events.
- The ground shaking at the site of the WAMO was simulated based on the recorded motions in Reston, Virginia, because to our knowledge no ground motions were recorded in the Washington, D.C., area during the 2011 Virginia earthquake. This indicates the importance of providing the U.S. east coast infrastructure with enough devices to record the seismic events of this region, in order to reduce the uncertainty associated with seismic motion estimation and to provide researchers with a comprehensive database with which to study the structural response in statistically predicted future events.

ACKNOWLEDGMENTS

The research described in this paper is supported by National Science Foundation grants CMMI-1219447, CMMI-1219473, and CMS-0402490 within the NEES (Network for Earthquake Engineering Simulation) Consortium Operation. Olgun is partly supported by the U.S. Geological Survey Earthquake Hazards Reduction Program under award G13AP00076. Godfrey is supported by National Science Foundation Graduate Research Fellowship Program grant DGE-0822220. We thank Robert Kayen (U.S. Geological Survey, Menlo Park, California) for providing soil profiles of the Washington Monument site and Ned Wallace

Downloaded from specialpapers.gsapubs.org on November 29, 2014

(National Park Service, Washington, D.C.) for his assistance in the field testing of the Washington Monument. The wired instrumentation system was partly provided by DIGITEXX Data Systems.

REFERENCES CITED

Allemang, R.J., 2003, The modal assurance criterion: Twenty years of use and abuse: Sound and Vibration Magazine, v. 37, no. 8, p. 14–23.

ASTM, 2010a, Standard C503/C503M–10—Standard Specification for Marble Dimension Stone: West Conshohocken, Pennsylvania, ASTM International, doi:10.1520/C0503_C0503M-10.

ASTM, 2010b, Standard C476–10—Standard Specification for Grout for Masonry: West Conshohocken, Pennsylvania, ASTM International, doi:10.1520/C0476-10.

ASTM, 2011, Standard C615/C615M–11—Standard Specification for Granite Dimension Stone: West Conshohocken, Pennsylvania, ASTM International, doi:10.1520/C615_C615M-11.

Chang, M., and Pakzad, S.N., 2013, Observer Kalman filter identification for output-only systems using Interactive Structural Modal Identification Toolsuite (SMIT): Journal of Bridge Engineering, v. 19, no. 5, doi:10.1061/(ASCE)BE.1943-5592.0000530.

Darton, N.H., 1951, Map showing the depth to bedrock in part of Washington, District of Columbia, Plate 2, *in* Darton, N.H., Configuration of the Bedrock Surface of the District of Columbia and Vicinity: U.S. Geological Survey Professional Paper 217, scale 1:16,800.

De Sortis, A., Antonacci, E., and Vestroni, F., 2005, Dynamic identification of a masonry building using forced vibration tests: Engineering Structures, v. 27, p. 155–165, doi:10.1016/j.engstruct.2004.08.012.

Gentile, C., and Saisi, A., 2007, Ambient vibration testing of historic masonry towers for structural identification and damage assessment: Construction & Building Materials, v. 21, p. 1311–1321, doi:10.1016/j.conbuildmat.2006.01.007.

Historic American Engineering Record, 1986, Washington Monument, Fifteenth Street between Independence & Constitution, Washington, District of Columbia: Washington, D.C., Library of Congress, http://www.loc.gov/pictures/item/dc0968/ (accessed June 2012).

John Milner Associates, Inc., 2004, Washington Monument and Associated Structures: Historic Structure Report for the National Park Service: Alexandria, Virginia, John Milner Associates, Inc., 486 p., http://www.nps.gov/history/history/online_books/wamo/wash_hsr1.pdf (accessed December 2012).

Oehrlein and Associates Architects, 1993, Evaluation of the Washington Monument for the National Park Service: Washington, D.C., Oehrlein and Associates Architects, 100 p., http://parkplanning.nps.gov/document.cfm?parkID=427&projectID=31299&documentID=43344 (accessed August 2012).

Washington Post, 2012, Monumental damage: 9 July 2012, http://www.washingtonpost.com/local/monumental-damage/2012/07/09/gJQAac3FZW_graphic.html (accessed November 2012).

Welch, P.D., 1967, The use of fast Fourier transform for the estimation of power spectra: A method based on time-averaging over short, modified periodograms: IEEE Transactions on Audio and Electroacoustics, v. 15, p. 70–73, doi:10.1109/TAU.1967.1161901.

Wiss, Janney, Elstner Associates, Inc., and Tipping Mar, 2011, Washington Monument post-earthquake assessment. Report for the National Park Service: http://www.nps.gov/wamo/upload/Post-Earthquake-assessment12_22_logo.pdf (accessed October 2012).

Manuscript Accepted by the Society 6 June 2014

Downloaded from specialpapers.gsapubs.org on November 29, 2014

Geological Society of America Special Papers Online First

Behavior and damage of the Washington Monument during the 2011 Mineral, Virginia, earthquake

S. Golnaz Shahidi, Shamim N. Pakzad, James M. Ricles, et al.

Geological Society of America Special Papers, published online November 26, 2014;
doi:10.1130/2015.2509(13)

E-mail alerting services click www.gsapubs.org/cgi/alerts to receive free e-mail alerts when new articles cite this article

Subscribe click www.gsapubs.org/subscriptions to subscribe to Geological Society of America Special Papers

Permission request click www.geosociety.org/pubs/copyrt.htm#gsa to contact GSA.

Copyright not claimed on content prepared wholly by U.S. government employees within scope of their employment. Individual scientists are hereby granted permission, without fees or further requests to GSA, to use a single figure, a single table, and/or a brief paragraph of text in subsequent works and to make unlimited copies of items in GSA's journals for noncommercial use in classrooms to further education and science. This file may not be posted to any Web site, but authors may post the abstracts only of their articles on their own or their organization's Web site providing the posting includes a reference to the article's full citation. GSA provides this and other forums for the presentation of diverse opinions and positions by scientists worldwide, regardless of their race, citizenship, gender, religion, or political viewpoint. Opinions presented in this publication do not reflect official positions of the Society.

Notes

© Geological Society of America

THE GEOLOGICAL SOCIETY OF AMERICA